

Task Aware Modulation using Representation Learning: An Approach for Few Shot Learning in Heterogeneous Systems

Arvind Renganathan* Rahul Ghosh* Ankush Khandelwal* Vipin Kumar*

Abstract

We present a Task-aware modulation using Representation Learning (TAM-RL) framework that enhances personalized predictions in few-shot settings for heterogeneous systems when individual task characteristics are not known. TAM-RL extracts embeddings representing the actual inherent characteristics of these entities and uses these characteristics to personalize the predictions for each entity/task. Using real-world hydrological and flux tower benchmark data sets, we show that TAM-RL can significantly outperform existing baseline approaches such as MAML and multi-modal MAML (MMAML) while being much faster and simpler to train due to less complexity. Specifically, TAM-RL eliminates the need for sensitive hyper-parameters like inner loop steps and inner loop learning rate, which are crucial for model convergence in MAML, MMAML. We further present an empirical evaluation via synthetic data to explore the impact of heterogeneity amongst the entities on the relative performance of MAML, MMAML, and TAM-RL. We show that TAM-RL significantly improves predictive performance for cases where it is possible to learn distinct representations for different tasks.

1 Introduction

In many real-world scenarios, we are interested in predicting the response of an entity/task given its drivers. For instance, consider the task of predicting Gross primary product (GPP) across the globe, where each grid cell is an entity. GPP measures the amount of carbon dioxide plants absorb through photosynthesis, which is driven by factors such as weather (e.g., temperature, rainfall) and Leaf Area Index (LAI). The relationship between drivers and response is often heterogeneous, as it is determined by entity characteristics. For example, different grid cells, defined by their ecoregions and climate zones, can have vastly different GPP responses to the same weather conditions and LAI values [18]. Such a scenario is quite common in environmental applications but can also be seen in other applications (e.g., people (entity) can have different heart rates (response)

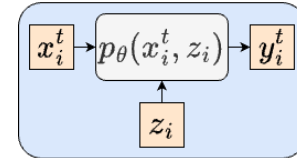


Figure 1: An abstract representation of a physical system, where x_i^t , y_i^t represent the input drivers, response, and z_i represents the entity characteristics of an entity i .

for the same physical activity (driver) depending on the physical fitness of the person (entity characteristic)). Figure 1 reflects this as an abstract scenario.

While such problems are often solved using process-based models [16], there is an increasing interest in using ML to address their well-known limitations [11, 32]. In particular, several works have already demonstrated the advantages of constructing an ML model that utilizes driver and response data from a set of well-observed entities (training set) and uses them to make predictions on entities that are not present in the training set in domains such as engineering [13], healthcare [19], and environmental sciences [16]. Typically, these “zero-shot” approaches require entity characteristics (also referred to as auxiliary characteristics) [31] to transfer information from the entities in the training set to those in the test set [15]. However, there are many situations where such auxiliary characteristics are either not available or highly uncertain [3].

This paper focuses on learning methods that can personalize predictions for each entity without any knowledge of the entity/task characteristics as long as it has a small amount of (driver, response) data (see Figure 2). This few-shot setting is in contrast to a traditional ML model that requires an ample amount of labeled (i.e., driver, response) data for each entity. Meta-learning [10] is a framework that enables models to quickly learn new tasks in a few-shot setting by leveraging task similarities.

Model agnostic meta-learning (MAML) [5] is one such approach that enables quick fine-tuning(adaptation) on new tasks with limited training data using a small number of gradient updates Fig 3a. The term “model-agnostic” in this context implies that these techniques are compatible with any base

*University of Minnesota. {renga016, ghosh128, khand035, kumar001}@umn.edu

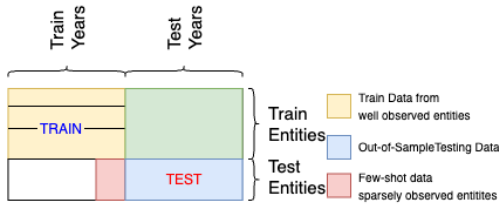


Figure 2: Experimental setting followed in this paper for testing. Modulation and adaptation are performed using few-shots of data when available

network trained via gradient descent. However, a single meta initialization for a base network does not work well when task distribution is multi-modal. Here, a commonly used approach is to train another network to generate entity-specific embeddings and use them to modulate a shared prediction network [2, 22, 28]. Multi-modal MAML (MMAML) is a prominent few-shot learning technique in this category.

Instead of learning a single meta-initialization point in the parameter space, MMAML first computes task-specific modulation parameters using its task modulation network, which includes a task encoder and a modulation parameter generator. Given this modulation parameter, MMAML then uses these parameters to modulate the meta-initialization of the base network. This meta-initialized base network is then meta-trained using a few steps of gradient-based adaptation towards the target case like MAML (see Figure 3b). However, there are several challenges; First, the adaptation step used during meta-training of the base network makes it less critical for MMAML to learn a high-quality modulation network. Second, backpropagating the gradients through the inner loop (with multiple updates) in MAML is difficult, and this problem worsens when using MAML in a multimodal meta-learning framework like MMAML because the gradient has to flow through not just the inner loop but also the modulation network. Together with the first challenge, this makes it even harder to learn a high-quality modulation. Finally, Additional issues affect MAML-like approaches, including instability depending on architectural and hyperparameter choices, lengthy training times, and the challenge of selecting the right hyperparameters.

This paper proposes a new multimodal meta-learning framework, Task Aware Modulation using Representation Learning (TAM-RL) to address these challenges. TAM-RL differs from MMAML in one key aspect: The modulated meta initializations are directly used for forward passes through the base network/model instead of another optimization procedures. This way of meta-learning is also termed amortized meta-learning, as the base and modulation networks are both trained in a unified fashion. This design choice in TAM-RL

addresses several issues in MMAML effectively. Firstly, TAM-RL’s modulation network is forced to learn meaningful representations, thereby generating improved meta-initializations for the base network. Secondly, by replacing inner-loop adaptation with a forward pass of the base network, TAM-RL achieves enhanced gradient propagation, resulting in a better-quality modulation network. Additionally, this design decision helps TAM-RL avoid problems commonly associated with MAML-like approaches, such as instability problems depending on the architecture and hyper-parameter choices, significant training times, and a cumbersome hyperparameter selection process, and relieves the need for second derivatives during training.

Our main contributions can be summarized as follows:

- We introduce *TAM-RL* as a novel multimodal Meta Learning framework for learning ML models for a diverse set of entities for a few-shot setting when explicit entity-specific characteristics are unknown.
- We perform an extensive evaluation of *TAM-RL* and existing relevant meta-modeling methods (e.g., MAML, MMAML) in predicting two important environmental problems of predicting Gross Primary Product (GPP) and forecasting streamflow in real-world datasets (section 3.1), demonstrating significantly better performance while being faster and much simpler to train due to reduced complexity.
- We present an empirical evaluation via synthetic data to explore the impact of heterogeneity amongst the entities on the relative performance of MAML, MMAML, and *TAM-RL*.

2 RELATED WORK

Few-shot Learning: In a Few-shot context, models are trained to accurately predict with very little labeled data per class or task. Recent successful methods use meta-learning to enable models to quickly learn from limited examples and effectively adapt to new tasks. One well-known method is MAML [5], which aims to find an initialization that allows a model to perform well on validation data after only a few inner adaptation steps. To handle multimodal task distributions, some studies [1, 28, 30] have proposed extending MAML to multiple initializations. They [2, 28] train another network to generate entity-specific embeddings and use them to modulate a shared meta-trained prediction network. However, although some studies have focused on applying these methods to time series regression, they do not address the core challenges of MMAML.

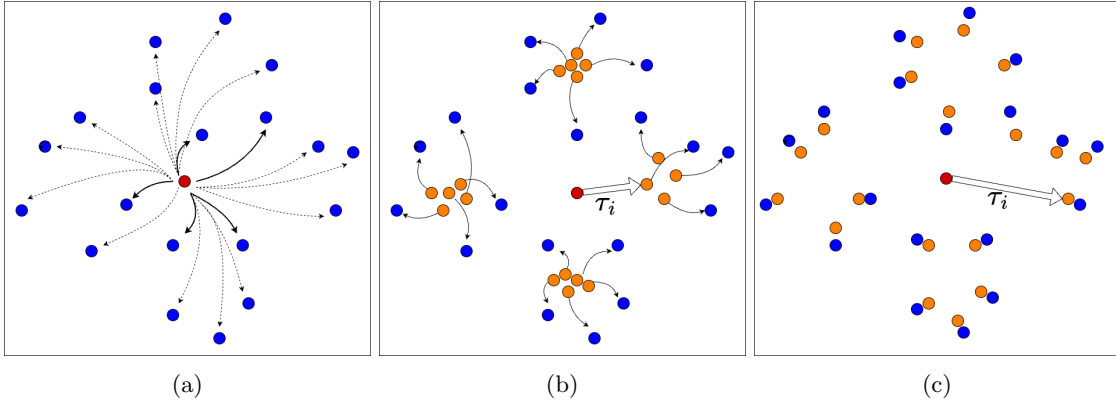


Figure 3: Comparing of MAML, MMAML and TAM-RL methods. a) MAML: Model computes shared initialization (red dot), which is adapted (curved arrows) to tasks (blue dots), it may fail to adapt to dissimilar tasks (outer blue dots) using few shots of data b) MMAML: Model uses task-specific modulation parameters to modulate (straight arrow) shared initialization (red dot) and get task specific initialization (orange dot) which are then adapted to tasks (blue dots). c) TAM-RL: Model uses task-specific modulation parameters to modulate (straight arrow) shared initialization (red dot) to directly compute meta initialization (orange dots) for given tasks (blue dots).

To solve its gradient, computation, and stability issues, one study [1] extended MMAML by switching the MAML trained base network to a simpler meta-learner, ProtoNet [25]. However, this restricts the meta-learner to only classification tasks and adopting them for regression-based tasks is nontrivial.

Neural processes (NP), another group of methods for the few-shot setting, combine Deep Neural Networks with Bayesian techniques like Gaussian Processes (GPs) to predict new functions while incorporating prior knowledge [6]. NPs use an inferred entity embedding to condition the prediction function on observed data. The model consists of an encoder for generating representations, an aggregator for merging representations, and a conditional decoder for creating target predictions [6]. This approach does not require the instantiation and maintenance of a unique set of model parameters, unlike computationally expensive MAML-based techniques that are sensitive to hyperparameter choices. However, to improve predictive performance, it is beneficial to jointly infer correlated tasks from multiple sources and leverage their underlying correlation [7, 12]. Ghosh et al. [7] introduced a specialized case of NP called KGSSL, which jointly infers time-invariant entity attributes from driver-response behavior and utilizes them to train a prediction model.

Multi-Task learning: The objective is to learn across multiple related tasks collectively. Collective learning across multiple tasks is achieved using sharing of some or all of their model parameters. This sharing of information allows the model to transfer knowledge between tasks [4]. Some examples of multi-task learning approaches are age group classification [10], mood prediction [26], human mobility prediction [29], streamflow

prediction [17]. However, the goal of MTL is to solve a fixed number of known tasks, unlike meta-learning, where the goal is often to solve unseen future tasks.

3 Problem Formulation

This study focuses on using ML models to learn driver-response behavior for various sparsely observed multi-modal entities. These entities can be physical systems like flux towers, river basins, tasks, people, or domains/distributions. We have access to a collection of driver/response pairs of time series sequences for each entity i in the train set. For each entity i in the Training set, we can access a set of multivariate time series instances of corresponding inputs and output pairs, $D_i^{Train} = [(\mathbf{X}_i^1, y_i^1), (\mathbf{X}_i^2, y_i^2), \dots, (\mathbf{X}_i^{T_{Train}}, y_i^{T_{Train}})]$, where The daily drivers \mathbf{X}_i are a multivariate time series, where $\mathbf{X}_i = [\mathbf{x}_i^1, \mathbf{x}_i^2, \dots, \mathbf{x}_i^T]$. where, $\mathbf{x}_i^t \in \mathbb{R}^{D_x}$ represents the input vector at time $t \in T$ with D_x dimensions, and $\mathbf{Y}_i = [y_i^1, y_i^2, \dots, y_i^T]$ represents the corresponding output.

Additionally, for the set of entities in the test set, a few-shot data of inputs and outputs, $D_j^{Few} = [(\mathbf{X}_j^1, y_j^1), (\mathbf{X}_j^2, y_j^2), \dots, (\mathbf{X}_j^{T_{Few}}, y_j^{T_{Few}})]$ is provided for each entity j .

The goal is to learn a regression function $\mathcal{F} : X \rightarrow Y$ that maps the input drivers to the output response for each entity in the test set. Individual ML models can be trained for each entity with sufficient training data. However, this is not feasible for many entities which lack sufficient training data. The behavior of entities is often governed by their inherent characteristics (z_i). Thus the forward model is represented as $\mathcal{F}_\theta(x_i^t, z_i)$, where θ denotes the function class shared by the target systems and z_i denotes entity-specific inherent characteristics.

The major challenge lies in handling the heterogeneity across different entities to achieve good performance over all entities, particularly in scenarios where the measurement of entity characteristics is unavailable. In this paper, we propose an entity-aware modeling approach to overcome the challenge of building a global model that can accurately predict the response of a new entity with limited observations, despite the heterogeneity across different entities.

Following the Meta-learning literature, we split the data for each entity into two sets: a support set ($D_i^{support}$) and a query set (D_i^{query}). For the entities used in training, both sets are taken from the training data (D_i^{train}). Whereas, for the entities in the test set, the few shot data (D_j^{few}) is used as the support set. During training, meta-learning approaches use the support set ($D_i^{support}$) to understand the temporal correlations, multivariate relationships, and task characteristics associated with each entity (i). This information is then used for prediction in the query set (D_i^{query}). The objective is to train the model on D_i^{train} by minimizing the prediction error:

$$(3.1) \quad \arg \min_{\theta} \sum_i \|y_i^t - \mathcal{F}(\mathbf{x}_i^t; D_i^{support})\|^2 \quad \text{where } (\mathbf{x}_i^t, y_i^t) \in D_i^{query}$$

3.1 Motivating Problems We apply our proposed framework to two important environmental problems: predicting Gross Primary Product (GPP) for flux towers with limited observations and forecasting streamflow in basins with sparse data. Both problems are important to address for practical reasons. Detailed high-resolution data is often lacking in regions such as the tropics and semi-arid areas, which are critical for the global carbon cycle. This data gap hampers our comprehensive understanding of the global carbon cycle, particularly in the context of climate change [21]. Additionally, enhancing streamflow predictions in areas with limited access to accurate streamflow measurements, especially in developing countries, can have substantial real-world impacts.

4 Method

The *TAM-RL* architecture has two major components, each serving a crucial purpose in the meta-learning process: 1) A Modulation network that consists of a BiLSTM-based task encoder \mathcal{E} , and a modulation parameter generator \mathcal{G} 2) A Base Network f_{θ} which is the prediction network. The Modulation network learns task-specific features representing the entity’s characteristics, which are then used to predict modulation parameters using a modulation parameter generator. The base network is modulated by these parameters to gen-

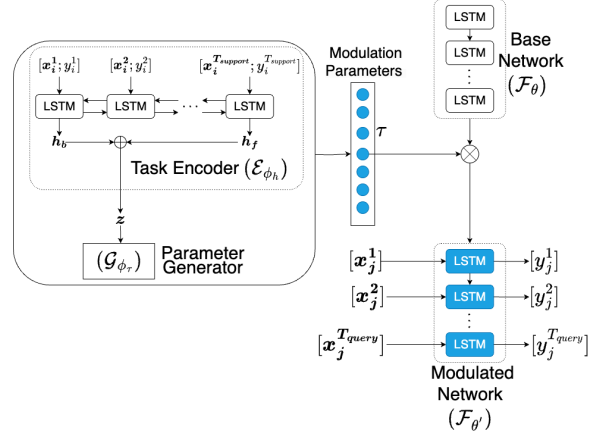


Figure 4: Model Architecture - The modulation network generates task-specific modulation parameters τ , which are subsequently utilized to adapt the base network for the target task. This diagram illustrates the architecture when the base network is an LSTM

erate modulated meta-parameters for the base network. The base network uses these Modulated meta parameters and input sequences to generate output sequences. During Inference, *TAM-RL* further uses an adaptation method that adjusts the base network to the specific task during inference. The following sections will provide more details on the neural network architectures used for *TAM-RL* and its training process.

4.1 Modulation Network

4.1.1 Task Encoder We use a Long Short-Term Memory (LSTM) network as a sequence encoder to capture the temporal information and relationship between the driver and response in sequences. LSTMs are ideal for tasks that involve long-range temporal dependencies and can solve problems with exploding and vanishing gradients. However, LSTMs only process sequences in the forward direction and do not provide insights into future data. To address this, we utilize a Bidirectional LSTM [8] based sequence encoder, which consists of two LSTMs (forward and backward) that generate embeddings for a sequence using the equations:

$$(4.2) \quad \begin{aligned} \mathbf{i}_t &= \sigma(\mathbf{W}_i [[\mathbf{x}^t; \mathbf{y}^t]; \mathbf{h}^{t-1}] + \mathbf{b}_i) \\ \mathbf{f}_t &= \sigma(\mathbf{W}_f [[\mathbf{x}^t; \mathbf{y}^t]; \mathbf{h}^{t-1}] + \mathbf{b}_f) \\ \mathbf{g}_t &= \sigma(\mathbf{W}_g [[\mathbf{x}^t; \mathbf{y}^t]; \mathbf{h}^{t-1}] + \mathbf{b}_g) \\ \mathbf{o}_t &= \sigma(\mathbf{W}_o [[\mathbf{x}^t; \mathbf{y}^t]; \mathbf{h}^{t-1}] + \mathbf{b}_o) \\ \mathbf{c}_t &= \mathbf{f}_t \odot \mathbf{c}_{t-1} + \mathbf{i}_t \odot \mathbf{g}_t \\ \mathbf{h}_t &= \mathbf{o}_t \odot \tanh(\mathbf{c}_t) \end{aligned}$$

To obtain the final embeddings (z), we add the last hidden states from both the forward (h_f) and backward LSTMs (h_b) in the Task encoder \mathcal{E} , as depicted in Fig 4. These task embeddings capture the temporal

information and interaction between the driver and the response for a given task.

$$(4.3) \quad \mathbf{z} = \mathcal{E}([x^t; y^t]_{1:T}; \phi_h)$$

where, \mathcal{E} is BilSTM with parameters ϕ_h .

4.1.2 Modulation Parameter Generator Modulation Parameter Generator is used to generate task-specific modulation parameters predict modulation parameters τ using the embedding vector of the task through an MLP layer. Afterward, we pass the learned embeddings through a multi-layer perceptron (MLP) layer to obtain the latent entity characteristics.

$$(4.4) \quad \tau = \mathcal{G}(\mathbf{z}; \phi_\tau)$$

where, \mathcal{G} is an MLP with parameters ϕ_τ .

4.2 Modulation For few-shot learning, it is essential to modulate the base network in a way that is parameter-efficient. Unconstrained modulation, while being flexible, can also be slow and prone to overfitting. Instead, we propose using Film modulation [24] of the LSTM gate outputs for LSTM-based base networks, and which requires only a small number of task-specific parameters for both real-world problems. We similarly also perform Film modulation at each layer for the fully connected neural network-based base network.

4.3 Base Network (Decoder) The Base Network can be any model trained with gradient descent and is customized architectural choices, unique to each domain and dataset, and analogous to forward models in the context of environmental modeling, thereby making TAM-RL model agnostic. We use an LSTM-based Base Network \mathcal{F} with modulated meta initialization to predict the response based on input drivers, as shown in the Base Network block of Fig 4, for our two real-life datasets for prediction of streamflow and GPP. The response is generated by a sequence-to-sequence LSTM network. Synthetic dataset uses a 4-layer fully connected neural network with ReLU non-linearity for each layer, as the base network. During Inference with TAM-RL, the modulation network is used to infer task-specific meta initialization of \mathcal{F} . The modulated base network is then optimized for the target task through gradient-based optimization, similar to MMAML [28].

4.4 Adaptation During Inference and not during training, the modulated base network is further optimized for the target task through gradient-based optimization, similar to MMAML [28]. We use an ADAM-based optimizer for the Adaptation step. It should be noted that the modulation network remains unaltered during the inference phase, preventing any negative impact from adaptation.

4.5 Training and Inference Algorithms To overcome the challenge of feeding a long time series into a model, we divide the training data (D^{Train}) into \mathcal{T} sliding windows ($W^{Tr\tau}$) during the training phase. These windows are further split into support windows ($W^{support\tau}$) and query windows ($W^{query\tau}$) for training the model. For each task in the support set, we select a support window ($W^{support\tau}$) from the Train($W^{Tr\tau}$) sliding windows and extract the corresponding response and driver data for the given entity. The query set is constructed similarly, with the remaining data that was not used to create the support set. This ensures that the model is trained on a diverse set of support tasks and can generalize to unseen tasks during inference. The entire framework is trained end to end using a forward loss, which can be any supervised loss, depending on the problem. In our experiments, we use mean squared error (MSE) as the supervised loss, as shown in equation 4.5.

$$(4.5) \quad \mathcal{L} = \frac{1}{N} \sum_{i=1}^N \frac{1}{T} \sum_{t=1}^T (y_i^t - \hat{y}_i^t)^2$$

The final objective of TAM-RL during training can be formally expressed as:

$$(4.6) \quad \arg \min_{\theta, \phi_h, \phi_\tau} \sum_i \|y_i^t - \mathcal{F}(\mathbf{x}_i^t; \theta'_i)\|^2 \quad \text{where} \quad \theta'_i = \theta_i \otimes \tau,$$

$$\tau = \mathcal{G}(\mathbf{z}; \phi_\tau),$$

$$\mathbf{z} = \mathcal{E}(W_i^{support\tau}, \phi_h),$$

$$s.t. (\mathbf{x}_i^t, y_i^t) \in W_i^{query\tau}$$

The pseudocode for the training process can be found in Algorithm 1 in supplementary section.

In the inference phase, we receive a small amount of data (D_j^{few}) for a new entity j , which we use to create \mathcal{T} support sliding windows ($W_j^{support\tau}$). These windows, along with the input data ($x_j^{query\tau}$), are used to make predictions. To do this, we first run a modulation network on a small amount of data to learn task-specific modulation parameters that modulate the base network. The modulated base network is then adapted using a few shots of Data. Finally, we use the task-specific characteristics, the input data, and the adjusted model parameters to make predictions. The detailed procedure is outlined in Algorithm 2 in the supplementary section.

5 Dataset & Baselines

5.1 Datasets

5.1.1 Flux Tower Dataset: FLUXNET2015 [23] dataset is a global network of 206 eddy-covariance stations that record carbon, water, and energy exchanges

between the atmosphere and the biosphere, offering valuable global-scale observations across various climate and ecosystem types. We aim to estimate Gross Primary Productivity (GPP) on a daily timescale for FLUXNET2015 sites using meteorological and remote sensing inputs (such as precipitation, air temperature, and vapor pressure.). In our study, we selected 150 towers with more than three years of data and divided them into training (145 sites) and test sets (15 sites), following guidelines outlined in [21]. We held out a year of data for the test sites to serve as the evaluation dataset. To evaluate our machine learning models on the held-out test year on test sites, we utilized limited years of data (ranging from one month to 24 months) for model adaptation from the "few-shot" data, as illustrated in Figure 2. For additional details on data preparation, please refer to the Appendix in supplementary section.

5.1.2 CARAVAN GB: CARAVAN is a global benchmark dataset comprising 6,830 basins from various open datasets worldwide, including regions such as the US, UK, GB, Australia, Brazil, and Chile. This dataset provides meteorological forcing data (e.g., precipitation, potential evaporation, temperature), streamflow observations, and basin characteristics. In this dataset, we aimed to estimate streamflow on a daily timescale for the CARAVAN GB Basins. We focused on a subset consisting of basins from the UK within CARAVAN, referred to as CARAVAN-GB, in our subsequent discussions. We selected a subset of 255 basins for our experiment, for which we had all streamflow observations between 1989 and 1999. The selection of train and test basins was based on mean streamflow, with a 4:1 ratio resulting in 204 basins for training and 51 basins for testing (test sites). We employed a k-fold approach (k=5) to evaluate all models' performance across all basins. The ML models were trained on train basins during train years and evaluated on out-of-sample basins during test years, which are not encountered during training, as shown in Fig 2. We assume we have access to a few-shot years of data for model performance evaluation.

5.1.3 Synthetic Dataset: We follow the synthetic data generation setup used by Vuorio et al. [28]. Specifically, we create a set of task distributions for regression with different modes. Modes are a collection of functions that include sinusoidal functions, linear functions, quadratic functions, ℓ_1 norm functions, and hyperbolic tangent functions. Each task/function from these modes is created by changing as shown:

Sinusoidal: $A \cdot \sin w \cdot x + b + \epsilon$, with $A \in [0.1, 5.0]$, $w \in [0.5, 2.0]$ and $b \in [0, 2\pi]$

Linear: $A \cdot x + b$, with $A \in [-3, 3]$

Quadratic: $A \cdot (x - c)^2 + b$, with $A \in [-0.15, -0.02] \cup [0.02, 0.15]$, $c \in [-3.0, 3.0]$ and $b \in [-3.0, 3.0]$

ℓ_1 norm: $A \cdot |x - c| + b$, with $A \in [-0.15, -0.02] \cup [0.02, 0.15]$, $c \in [-3.0, 3.0]$ and $b \in [-3.0, 3.0]$

Hyperbolic tangent: $A \cdot \tanh(x - c) + b$, with $A \in [-3.0, 3.0]$, $c \in [-3.0, 3.0]$ and $b \in [-3.0, 3.0]$

We add Gaussian noise ($\mu = 0$ and standard deviation = 0.3) to each data point obtained from the individual task.

5.2 Baselines & Implementation Details

- **MAML:** We train a global model using MAML [5] as the baseline to compare with existing methods. For our real-world dataset, MAML uses LSTM as the base network. It uses a 4-layer fully connected neural network for synthetic datasets with ReLU non-linearity for each layer. The architecture of MAML on each individual dataset is designed to be the same as base network in TAM-RL
- **MMAML:** We train a global model using MMAML [28] as the baseline to compare with existing methods. For our real-world dataset, MMAML uses BiLSTM and MLP for the task encoder and Modulation Parameter Generator in the modulation network and LSTM as the base network. For the synthetic dataset, MMAML uses BiLSTM and MLP as the modulation network and a 4-layer fully connected neural network with ReLU non-linearity for each layer as the base network. MMAML(w/o)adapt is the version of MMAML obtain pre-adaptation step in inference. The architecture of MMAML on each individual dataset is designed to be the same as base network and modulation network in TAM-RL

6 Experimental and Results

6.1 Real World Datasets This section presents the results of two experiments conducted on real-world datasets: the Flux Tower Dataset and the CARAVAN GB Dataset. For the Flux Tower Dataset, we preprocess time series data by creating sliding windows of 30 days, strided by half the sequence length (15 days). The LSTM base network takes 30-length sequences as input and generates output at a stride of 15 days. Similarly, we create sliding windows of 365 days for the streamflow dataset, strided by half the sequence length (183 days). Here, LSTM takes 365-length sequences as input and generates output at a stride of 183 days.

We compare the performance of our proposed method, TAM-RL, with two baseline methods, MAML and MMAML, in a few-shot learning setting. Both datasets utilize LSTM designed as a sequence-to-

Architecture	Flux Tower (in Months)								Caravan-GB (in Years)					
	1		3		12		24		1		2		5	
	PM	PA	PM	PA	PM	PA	PM	PA	PM	PA	PM	PA	PM	PA
MAML	-	2.71	-	2.54	-	2.13	-	2.12	-	1.40	-	1.39	-	1.38
MMAML	7.09	2.77	6.39	2.65	6.22	2.07	6.03	1.95	1.72	1.35	1.72	1.34	1.72	1.29
TAM-RL (ours)	2.38	2.39	2.35	2.31	2.20	1.79	2.19	1.73	1.45	1.29	1.29	1.23	1.25	1.19

Table 1: Mean Ensemble Root Mean Square Error (RMSE) for GPP prediction flux tower dataset and streamflow modeling on CARAVAN-GB Benchmark dataset, comparing TAM-RL and the baselines Post Modulation (PM) and Post Adaptation(PA). The amount of data used as few-shots are denoted as column names.

sequence prediction as base networks, chosen for their ability to handle sequential inputs and generate predictive outputs. For both datasets, we employ BiLSTM and an MLP layer for the modulation network, representing the task encoder and Modulation Parameter Generator, respectively. The best training hyperparameters differ by domain of application and baseline method. Please refer to the supplementary materials for concrete specifications of the best hyperparameters. To mitigate the impact of randomness due to network initializations, we report results of the ensemble prediction obtained by averaging the predictions of five models with different weight initializations for all architectures (ours and baselines).

Table 1 presents the mean ensemble RMSE values for GPP prediction in the Flux Tower Dataset and streamflow prediction in the CARAVAN-GB Benchmark datasets. The columns in the table represent the available few-shot observation data for modulation and adaptation (see Figure 2 for experimental setting). For All architectures, we report performance evaluation post Adaptation; for models with a modulation network (MMAML and TAM-RL), we also provide performance evaluation Post Modulation(i.e., Pre-Adaption) to evaluate the modulation network.

From Table 1, we observe that MAML’s overall performance remains relatively weak, showing that a single initialization is challenging to adapt for all target tasks. For GPP prediction in flux tower, we observe that MMAML post-modulation struggles without the adaptation step but is able to improve its performance significantly (by a margin of 155-209 %) under different few-shot situations) post adaptation. Similar behavior is observed in streamflow prediction, where MMAML is able to improve its performance significantly once adapted(21.6 to 25%). This behavior aligns with MMAML’s expected behavior, as it is designed to exhibit enhanced performance when adapted using a few-shots of data during testing. In contrast, TAM-RL performs comparable to or better than MAML and MMAML even without adaptation. Furthermore, in streamflow modeling, TAM-RL, without adaptation but modulated using two years of few-shot data, outperforms both baselines post-modulation and adaptations.

For GPP prediction, TAM-RL, without adaptation, demonstrates a remarkable trend of performance improvement as the number of few-shot years of data increases. This illustrates TAM-RL’s capacity to effectively leverage additional data points, resulting in improved modulation parameters. Furthermore, when TAM-RL performs both modulation and adaptation with limited observations, it demonstrates performance improvements compared to TAM-RL without adaptation. While part of this improvement can be attributed to a better base network, most of the enhancements are driven by the modulation of task-specific parameters. In contrast, for GPP prediction MMAML’s performance gains with increasing few-shot data are primarily influenced by the adaptation process using the available few-shot data for adjusting the base network. These observations hold true for the streamflow prediction dataset as well.

TAM-RL outperforms our primary baseline, Multimodal MAML (*MMAML*), by a substantial margin for GPP flux prediction. It achieves a 13.7% improvement with 1 month of few-shot data, 12.8% with three months of few-shot data, 13.5% with 12 months of few-shot data, and 11.3% improvement with 24 months of few-shot data. Similar improvements can be observed for streamflow prediction where TAM-RL outperforms our primary baseline, Multi-Model MAML (*MMAML*), by a substantial margin. It achieves an 8.21% improvement with two years of data and a 7.8% improvement with five years of data. Additionally, TAM-RL is 10 times faster in terms of training time. This is because MMAML has $N \times A$ backpropagation operations to the forward model (An adaptation for each task individually) per batch. In comparison, *TAM-RL* performs only one backpropagation operation, significantly reducing training time while being easy to optimize because it has two less crucial hyperparameters than MMAML.

6.2 Experiment: Synthetic Dataset with Multiple Modes (sinusoidal, tanh, linear, quadratic, ℓ_1 norm) We further evaluate *TAM-RL* using a synthetic dataset to understand in what situation *TAM-RL* outperforms *MMAML* and vice-versa. We create three sets of multimodal task distribution with varying

Architecture	SET_1 {Sin, Linear, Quadratic}	SET_2 {Linear, Tanh, ℓ_1 norm}	SET_3 {Quadratic, Tanh, ℓ_1 norm}
MAML	3.684 (0.176)	3.446 (0.115)	1.454 (0.040)
MMAML	0.601 (0.074)	1.085 (0.121)	0.757 (0.05)
<i>TAM-RL</i> (ours)	0.494 (0.040)	1.049 (0.69)	0.805 (0.023)

Table 2: Mean square error (MSE) on the multimodal 5-shot regression with different combinations of 3 modes for different architectures across different sets. Gaussian noise is applied to each function with $\mu = 0$ and $\sigma = 0.3$. Values in brackets represent the standard deviation across tasks in the set

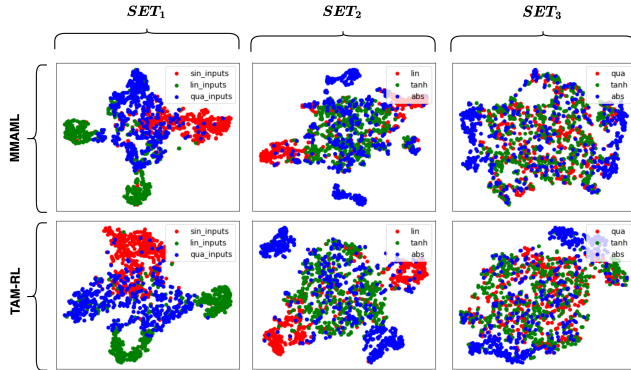


Figure 5: tSNE plots of the task embeddings produced by *MMAML* (top row) and *TAM-RL* (bottom row) for the three sets of multimodal tasks (shown in columns).

levels of mode similarity. Each set consists of three different families of functions (modes), as shown below:

- SET_1 : {Sine, Linear, Quadratic}
- SET_2 : {Linear, Tanh, ℓ_1 norm}
- SET_3 : {Quadratic, Tanh, ℓ_1 norm}

SET_1 has the most distinct tasks (hence, it would be possible to learn distinct representations for each task), and SET_3 has the least separable tasks (making it harder to learn distinct representations for each task). We select 375,000 tasks for each family of functions (task modes), and each task has five meta-train and five meta-validation examples for training. For batching, we sample them uniformly by selecting 25 tasks from each task mode in a batch, leading to a total of $3 \times 25 = 75$ tasks for each batch and a total of 15000 batches for each set. To evaluate each set, we sample 12,500 new tasks for each family of functions (task mode), which equals 37,500 new tasks for the whole set.

We train a *MAML*, *MMAML*, and *TAM-RL* for each of the above three sets of multimodal distributions. Following [28], we use an MLP-based base network for all three models *MAML*, *MMAML*, *TAM-RL*. For *MMAML* and *TAM-RL*, Bidirectional LSTM is used as the task encoder. Please refer to the appendix for details of the architecture. We use ADAM as the meta-optimizer and use the same hyperparameter settings as the regression experiments in [28]. We evaluate all models with five gradient steps during adaptation using

five meta-train examples for these new tasks. As the evaluation criterion, we report the mean squared error (MSE) of five meta-validation examples of these new tasks.

Fig 5 show the tSNE plots [27] of the task embeddings produced by *TAM-RL* and *MMAML*, respectively, from randomly sampled tasks for each set. From the tSNE plot, we observe that as we move from SET_1 to SET_3 , the class of functions becomes more and more homogeneous. For example, a quadratic function can resemble a sinusoidal or linear function, but generally, a sinusoidal function is dissimilar from a linear function. SET_3 is homogenous because quadratic, ℓ_1 , and hyperbolic tangent functions are very similar, particularly with Gaussian noise in the output space. Further, we can observe from the tSNE plots that *TAM-RL* and *MMAML* task embeddings generate similar tSNE plots and clusters.

The quantitative results for all three sets are shown in Table 2. For each architecture, we report the mean MSE for the set. We can observe that SET_1 has a reasonably heterogeneous split, as shown in Fig 5. For SET_1 , the performance of *TAM-RL* is 21.6% better than *MMAML*. As the set becomes more homogenous, like in SET_2 , the performance gap between *TAM-RL* and *MMAML* narrows and, in this scenario, *TAM-RL* only holds a slight edge of 3.5% over *MMAML*, and they operate at a similar performance level. When the dataset reaches complete homogeneity, as in SET_3 , *TAM-RL* achieves similar performance to *MMAML*_{Adapt}. From Table 2, we can also observe that MAML has the highest error in all settings and that incorporating task identity through task embeddings matters significantly in multimodal task distributions. This shows that *TAM-RL* outperforms *MMAML* as the set becomes more heterogeneous. *MMAML*'s task encoder is not able to capture the heterogeneous task structure and thus provides suboptimal results. The design choice of *TAM-RL*, which leverages meta-initializations directly without needing an adaptation phase, proves highly effective when tasks have distinct characteristics, allowing the modulation network to learn meaningful representations for generating superior meta-initializations.

7 Conclusion

This paper presented TAM-RL a novel task-aware modulation framework using representation learning learning, for use in a few shot setting. We performed extensive experiments on two real-world environmental datasets, a GPP predictions task for flux towers and hydrological benchmark dataset CARAVAN GB, showing that this framework *TAM-RL* outperforms baseline models for less-observed entities. We further showed that *TAM-RL* outperforms MMAML when multimodal task distribution is more heterogeneous. To summarize, *TAM-RL*'s approach of doing a forward pass instead of an adaptation phase in training shows non-trivial improvements in multiple aspects and has the potential to impact many personalized prediction applications. Our proposed method is general and can add value in other applications where global models are to be learned in a setting with a diverse set of entities, where only a few shots of information are available for a new entity. As presented, our framework cannot handle missing driver or response data observations. However, this methodology can be further extended to handle missing observations. KGSSL [7] showed that incorporating Knowledge-guided Self-Supervised Learning into their task encoder improved their prediction performance as now the task embeddings had semantic meaning. One potential research direction is incorporating similar knowledge guidance into our methodology. The code used in this paper is available at Google Drive ¹.

References

- [1] Milad Abdollahzadeh et al. Revisit multimodal meta-learning through the lens of multi-task learning. *NeurIPS*, 2021.
- [2] Sebastian Pineda Arango et al. Multimodal meta-learning for time series regression. In *International Workshop on Advanced Analytics and Learning on Temporal Data*, 2021.
- [3] Keith Beven. Deep learning, hydrological processes and the uniqueness of place. *Hydrological Processes*, 2020.
- [4] Rich Caruana. Multitask learning. *Machine learning*, 1997.
- [5] Chelsea Finn et al. Model-agnostic meta-learning for fast adaptation of deep networks. In *ICML*, 2017.
- [6] Marta Garnelo et al. Neural processes. *arXiv*, 2018.
- [7] Rahul Ghosh et al. Robust inverse framework using knowledge-guided self-supervised learning: An application to hydrology. *KDD '22*, 2022.
- [8] Alex Graves et al. Frameworkwise phoneme classification with bidirectional lstm networks. In *IJCNN*, 2005.
- [9] Hans Hersbach et al. The era5 global reanalysis. *Quarterly Journal of the Royal Meteorological Society*, 146(730):1999–2049, 2020.
- [10] Timothy Hospedales et al. Meta-learning in neural networks: A survey. *TPAMI*, 2021.
- [11] Xiaowei Jia et al. Physics guided rnns for modeling dynamical systems: A case study in simulating lake temperature profiles. *SDM*, 2019.
- [12] Donggyun Kim et al. Multi-task neural processes. *arXiv:2110.14953*, 2021.
- [13] Young-Min Kim et al. Predictive modeling for machining power based on multi-source transfer learning in metal cutting. *IJPEM - Green Tech*, 2022.
- [14] Diederik P Kingma et al. Adam: A method for stochastic optimization. *ICLR*, 2015.
- [15] Frederik Kratzert et al. Toward improved predictions in ungauged basins: Exploiting the power of machine learning. *Water Resources Research*, 2019.
- [16] Frederik Kratzert et al. Towards learning universal, regional, and local hydrological behaviors via machine learning applied to large-sample datasets. *HESS*, 2019.
- [17] Xiang Li et al. Regionalization in a global hydrologic deep learning model: From physical descriptors to random vectors. *Water Resources Research*, 2022.
- [18] Shangrong Lin et al. Improved global estimations of gross primary productivity of natural vegetation types by incorporating plant functional type. *Int. J. Appl. Earth Obs. Geoinf.*, 2021.
- [19] Yash-ye Logan et al. Patient aware active learning for fine-grained oct classification. *ICIP*, 2022.
- [20] R. Myneni et al. Mod15a2h modis/terra leaf area index/fpar 4-day 14 global 500m sin grid v006 [data set]. *NASA EOSDIS Land Processes Distributed Active Archive Center*, 23:2023–09, 2015.
- [21] Juan Nathaniel et al. Metaflux: Meta-learning global carbon fluxes from sparse spatiotemporal observations. *Scientific Data*, 2023.
- [22] Boris Oreshkin et al. Tadam: Task dependent adaptive metric for improved few-shot learning. *NeurIPS*, 2018.
- [23] Gilberto Pastorello et al. The fluxnet2015 dataset and the oneflux processing pipeline for eddy covariance data. *Scientific data*, 2020.
- [24] Ethan Perez et al. Film: Visual reasoning with a general conditioning layer. In *AAAI*, 2018.
- [25] Jake Snell et al. Prototypical networks for few-shot learning. *NeurIPS*, 30, 2017.
- [26] Sara Taylor et al. Personalized multitask learning for predicting tomorrow's mood, stress, and health. *IEEE Transactions on Affective Computing*, 2017.
- [27] Laurens Van der Maaten et al. Visualizing data using t-sne. *JMLR*, 2008.
- [28] Risto Vuorio et al. Multimodal model-agnostic meta-learning via task-aware modulation. *NeurIPS*, 2019.
- [29] Haoxiang Wang et al. Bridging multi-task learning and meta-learning: Towards efficient training and effective adaptation. In *ICML*, 2021.

¹https://drive.google.com/drive/folders/1Z_Uuq6qEzCkaiPYAtPapgEiIZzZnXxy

- [30] Ruohan Wang et al. Structured prediction for conditional meta-learning. *NeurIPS*, 2020.
- [31] Wei Wang et al. A survey of zero-shot learning: Settings, methods, and applications. *ACM Transactions on Intelligent Systems and Technology (TIST)*, 2019.
- [32] Jared Willard et al. Integrating scientific knowledge with machine learning for engineering and environmental systems. *ACM Computing Surveys*, 2022.

Appendix

7.1 Dataset Details

7.1.1 Fluxtower Dataset The FLUXNET2015 [23] dataset is a global network of eddy-covariance stations that record carbon, water, and energy exchanges between the atmosphere and the biosphere. It offers valuable ecosystem-scale observations across various climate and ecosystem types. In this dataset, our goal is to estimate Gross Primary Productivity (GPP) on a daily timescale for FLUXNET2015 sites. We achieve this by using a combination of meteorological and remote sensing inputs, including precipitation, 2-meter air temperature (T_a), vapor pressure deficit (VPD), incoming short-wave radiation from ERA5 reanalysis data [9], and Leaf Area Index (LAI) data from MODIS [20]. We extract the time series data closest to each tower site, following a similar approach to [21].

Out of the 206 flux towers in the FLUXNET2015 dataset, we selected 150 towers with data spanning more than three years. We considered the most recent three years of data for each selected flux tower for analysis. These towers were divided into training and test sets, following guidelines outlined in [21]. This process involved selecting half of the towers from tropical and semi-arid regions, which are typically sparse, and one tower from each plant functional type (PFT), including those within cropland and boreal areas, for testing (15 sites). The remaining towers constituted the training set (145 sites). Additionally, we further divided the test site data into two blocks: a two-year block representing different scenarios of "few-shot" data availability for testing purposes and one one-year block held out set for testing.

To evaluate our machine learning models on the held-out test year on test sites, we utilized limited years of data (ranging from one month to 24 months) for model adaptation from the "few-shot" data, as illustrated in Figure 2.

7.1.2 CARAVAN-GB CARAVAN is a recent global benchmark dataset comprising 6,830 basins from various open datasets worldwide, including regions such as the US, UK, GB, Australia, Brazil, and Chile. This dataset provides meteorological forcing data (e.g., precipitation, potential evaporation, temperature), streamflow observations, and basin characteristics. For our study, we focused on a subset consisting of 408 basins from the UK within CARAVAN, referred to as CARAVAN-GB in our subsequent discussions. In this dataset, our goal was to estimate streamflow on a daily timescale for CARAVAN GB Basins. Table 3 shows the meteorological forcing

data used in our real-world hydrology experiment with CaravanGB. Our study analyzed data spanning from October 1st, 1989, to September 30th, 2009. The model training phase employed data from 1989 to 1999, while the testing phase encompassed the years 1999 to 2009. The training period from 1989 to 1999 was further divided into training years (1989-1997) and validation years (1997-1999). Out of the 408 available Basins in CARAVAN-GB, we selected 255 basins for our experiment based on the absence of missing streamflow observations between 1989 and 1999. The experimental setting, depicted in Fig 2, involved dividing the basins into train and test sets. The ML models were trained on train basins during train years. The selection of train and test basins was based on mean streamflow, with a 4:1 ratio resulting in 204 basins for training and 51 basins for testing (test sites). We employed a k-fold approach ($k=5$) to evaluate all models' performance across all basins. For model performance evaluation, the test set employed limited years of data (one year, two years, five years) from the training period, as depicted in Fig 2, for fine-tuning and inferring characteristics as needed within the model. We evaluate on out-of-sample testing blocks as shown in experimental setting Fig 2.

Meteorological forcing data	Unit
Daily Precipitation sum(total_precipitation_sum)	mm/day
Daily Potential evaporation sum(potential_evaporation_sum)	mm/day
Mean Air temperature (temperature_2m_mean)	$^{\circ}C$
Mean Dew point temperature (dewpoint_temperature_2m_mean)	$^{\circ}C$
Mean Shortwave radiation (surface_net_solar_radiation_mean)	Wm^{-2}
Mean Net thermal radiation at the surface (surface_net_thermal_radiation_mean)	Wm^{-2}
Mean Surface pressure (surface_pressure_mean)	kPa
Mean Eastward wind component (u_component_of_wind_10m_mean)	ms^{-1}
Mean Northward wind component (v_component_of_wind_10m_mean)	ms^{-1}

Table 3: A table of meteorological forcing data used in this experiment.

7.2 Hyperparameter Tuning

Hyperparameter	Value
Dimension of Encoder	16, 32, 64
Dimension of hidden state for Forward Model	128, 256, 350 , 500
Batch size	32 , 64 , 128
Learning rate	0.005, 0.001 , 0.0005, 0.01

Table 4: Range of parameter values tried for hyperparameter tuning, with the final selected value shown in **bold**.

7.2.1 Experiment: Flux Tower Dataset To find the best hyperparameters, we performed a grid search across a range of parameter values. The possible values considered are listed in Table 5. We trained our model, *TAM-RL*, using data from training sites. The final hyperparameters, including batch size and learning rates, are determined after performing a k-fold cross-validation ($k=5$) on the training set. Finally, we evaluated the model's performance on the testing sites

during the hold out test period, as shown in Figure 2.

Hyperparameter	Value
Latent dimension of Encoder	16, 32 , 64
Dimension of hidden state for Forward Model	64, 128 , 256
Batch size	32, 64 , 128
Learning rate	0.005, 0.001 , 0.0005, 0.01

Table 5: Range of parameter values tried for hyperparameter tuning, with the final selected value shown in **bold**.

7.2.2 Experiment: CARAVAN GB To find the best hyperparameters, we performed a grid search across a range of parameter values. The possible values considered are listed in Table 5. We trained our model, *TAM-RL*, using data from the training basins during the training period. The final hyperparameter configuration was chosen based on the set with the lowest average RMSE in the validation period for the training basins. Finally, we evaluated the model’s performance on the testing basins during the test period, as shown in Figure 2.

7.2.3 Experiment: Synthetic Dataset We use the same hyperparameter settings as the regression experiments presented in [28] and used Adam [14] as the meta-optimizer.

7.3 Network Architectures

7.3.1 Base Network For the Flux Tower Dataset, we use an LSTM as the base network with hidden dimension of 350; for the Caravan-GB dataset, we use an LSTM as the base network with a hidden dimension of 128. For the synthetic dataset, Like in the case of [28], we use a 4-layer fully connected neural network with a hidden dimension of 100 and ReLU non-linearity for each layer as a base network.

7.4 Task Encoder We use a BiLSTM as the base network for all three datasets, where Flux towers BiLSTM uses 64 hidden dimensions, Caravan-GB uses a BiLSTM of 32 hidden dimensions and the synthetic dataset uses BiLSTM of hidden dimension 40.

7.5 Modulation For few-shot learning, it is essential to modulate the base network in a way that is parameter-efficient. Unconstrained modulation, while being flexible, can also be slow and prone to overfitting. Instead, we propose using Film modulation [24] of the LSTM gate outputs for LSTM-based base networks, and which requires only a small number of task-specific parameters for both real-world problems. We similarly also perform Film modulation at each layer for the fully

connected neural network-based base network.

7.6 Parameter Generator All models have an MLP layer as a parameter generator. Since the task network of Flux tower dataset is an LSTM. LSTM has four gates, so according to our modulation strategy, we employ four linear fully-connected layers to convert the task embedding vector z to a vector of hidden dimension 700 ie $4*(64,700)$, as the hidden dimension of the LSTM base network was 350 and for film modulation we need twice of hidden dimension as in our implementation we use half the dimension of the vector as two components for FILM modulation. Similarly, the Hydrology dataset also uses an LSTM as a base network. So we use four linear fully connected layers of dim (32,256). The synthetic dataset has four convolutional layers with channel sizes 32, 64, 128, and 256 so to modulate them we create four linear layers with output dimensions of 64,128,256,512 respectively.

7.7 Ablation: CARAVAN GB The *TAM-RL* architecture consists of three major components: a BiLSTM-based task encoder, an LSTM decoder-based forward model, and an adaptation method. The task encoder is responsible for learning the task-specific features of the input data. The forward model generates the output sequence given the input sequence and task-specific features. The adaptation method, along with the task embeddings from the task encoder, adapts the forward model to the specific task during inference. There are several possible ablations of the *TAM-RL* architecture. One ablation would be to remove the task encoder and adaptation method resulting in a simple LSTM-based global model. Another ablation would be to add an LSTM encoder to the previous ablation without the adaptation step resulting in a model with two LSTM layers, one for the task encoder and one for the forward model. A third ablation would be to switch the task encoder from LSTM to BiLSTM (this is the same as *TAM-RL* in Table 1). The next three possible ablations would be adding adaptation steps to the above-described models. All six possible ablations are shown in Table 6. There are several key observations to be made. Firstly, models equipped with an encoder consistently exhibit superior performance compared to those lacking an encoder block. Secondly, among the encoder block options, Bi-LSTM outperforms LSTM, thus proving to be a more effective choice. Lastly, a crucial observation is that adaptation consistently contributes to improved results.

7.8 Pseudocode

Ablation	Method in Table1	0 Years	2 Years	5 Years
No Encoder No Adapt	LSTM	0.18	0.18	0.18
LSTM Encoder no Adapt	Not in Table 1	N/A	0.55	0.55
BiLSTM Encoder no Adapt	<i>TAM-RL</i>	N/A	0.57	0.57
No Encoder with Adapt	LSTMAdapt	0.18	0.32	0.41
LSTM Encoder with Adapt	Not in Table 1	N/A	0.59	0.62
BiLSTM Encoder with Adapt	<i>TAM-RLAdapt</i>	N/A	0.63	0.63

Table 6: Ablation study for the Caravan-GB out of sample testing. Numbers in the table show NSE values(Higher is better).

7.8.1 Training Algorithm Algorithm 1 shows the training procedure followed in TAM-RL.

Algorithm 1 *TAM-RL* Training Algorithm

Require: $W^{Tr\tau} = [W^{support\tau}, W^{query\tau}]$ generated from D^{Train} , α : step size hyper-parameter; We abbreviate support as s and query as q

- 1: Randomly Initialize the pipeline with weights θ , ϕ_{tau} and ϕ_h
- 2: **for** epoch = 1 to N **do**
- 3: **while** not Done **do**
- 4: Sample batches of entities $W_k^{Tr\tau} \sim W^{Train\tau}$
- 5: **for** all k **do**
- 6: Infer $z = \mathcal{E}(W_k^{s\tau}; \phi_h)$
- 7: Infer $\tau = \mathcal{G}(z; \phi_\tau)$
- 8: Update θ , ϕ_{tau} and ϕ_h with $\alpha \nabla_{\theta, \omega} \mathcal{L}_{W_k^{Tr\tau}}(\mathcal{F}(x_k^{qt}; \theta, \tau); W_k^{q\tau})$
- 9: **end for**
- 10: **end while**
- 11: **end for**

7.8.2 Inference Algorithm Algorithm 2 shows the inference procedure followed in TAM-RL.

Algorithm 2 *TAM-RL* Inference Algorithm

Require: $W_j^{support\tau}$ generated from D_i^{Few} , x_j^{queryt} , β : step size hyper-parameter, num_inner_steps: no. of gradient steps for the inner loop; We abbreviate support as s and query as q

Ensure: Output y_j^{qt} for input driver x_j^{qt} of an entity j

- 1: load θ , ϕ_{tau} and ϕ_h from trained model
- 2: Infer $z = \mathcal{E}(W_j^{s\tau}; \phi_h)$
- 3: Infer $\tau = \mathcal{G}(z; \phi_{tau})$
- 4: **for** epoch = 1 to num_inner_steps **do**
- 5: Update θ with $\beta \nabla_{\theta} \mathcal{L}_{W_j^{s\tau}}(\mathcal{F}(x_j^{st}; \theta, \tau); W_j^{s\tau})$
- 6: **end for**
- 7: **return** $y_j^{qt} = (\mathcal{F}(x_j^{qt}; \theta, \tau))$

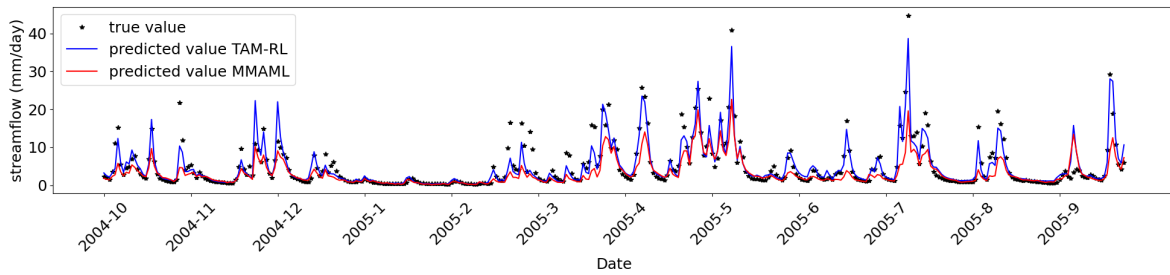
7.9 Streamflow Prediction Plot Figure 6a shows the prediction from the models without adaptation. We can observe that the *TAM-RL* predictions match the observed streamflow better than *MMAML*. Figure 6b shows the prediction from the models on adapting with

only two years of data. From the plot, we observe that all models' prediction improves in general. However, *TAM-RL* gives a prediction closer to the ground truth.

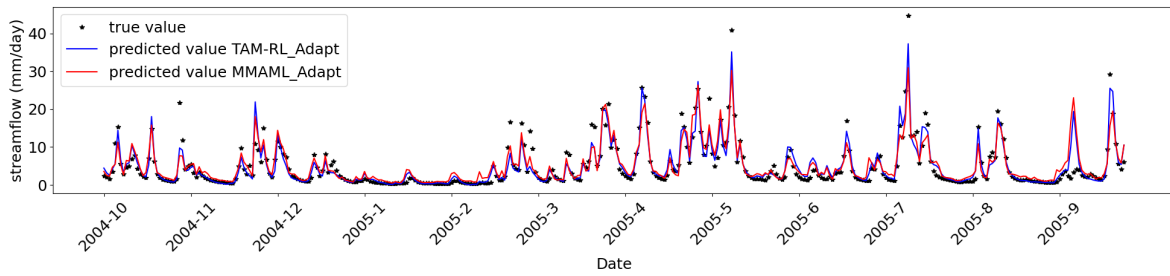
7.10 Reproducibility CARAVAN dataset is freely available at zenodo at ². The code used in this paper is available at Google Drive ³.

²<https://doi.org/10.5281/zenodo.7540792>

³https://drive.google.com/drive/folders/1Z_Uuq6qEzCkaiPYAtPapgEiIZzZnXxy



(a)



(b)

Figure 6: Observed Streamflow and predicting streamflow by different model architectures a) Models w/o adaptations b) Models with adaptations (Best seen in color)